SUB-AMBIENT CONTROLLED TURBULENCE EFFECTS ON DISCHARGE STABILIZATION FOR LASER APPLICATIONS

Naval Postgraduate School,
Monterey, California

September 1976

335114

NW

NAVAL POSTGRADUATE SCHOOL
Monterey, California

THESIS

SUB-AMBIENT CONTROLLED TURBULENCE
EFFECTS ON DISCHARGE STABILIZATION FOR
LASER APPLICATIONS

by

Howard Allen Post

September 1976

Thesis Advisor: Oscar Biblarz

Approved for public release; distribution unlimited.

REPORT DOCUMENTATION PAGE		READ INSTRUCTIONS BEFORE COMPLETING FORM
1. REPORT NUMBER	2. GOVT ACCESSION NO.	3. RECIPIENT'S CATALOG NUMBER
4. TITLE (and Subtitle) Sub-Ambient Controlled Turbulence Effects on Discharge Stabilization for Laser Applications		5. TYPE OF REPORT & PERIOD COVERED Master's Thesis September 1976
		6. PERFORMING ORG. REPORT NUMBER
7. AUTHOR(s) Howard Allen Post		8. CONTRACT OR GRANT NUMBER(s)
9. PERFORMING ORGANIZATION NAME AND ADDRESS Naval Postgraduate School Monterey, California 93940		10. PROGRAM ELEMENT, PROJECT, TASK AREA & WORK UNIT NUMBERS
11. CONTROLLING OFFICE NAME AND ADDRESS Naval Postgraduate School Monterey, California 93940		12. REPORT DATE September, 1976
		13. NUMBER OF PAGES 64
14. MONITORING AGENCY NAME & ADDRESS(if different from Controlling Office) Naval Postgraduate School Monterey, California 93940		15. SECURITY CLASS. (of this report) Unclassified
		15a. DECLASSIFICATION/DOWNGRADING SCHEDULE

16. DISTRIBUTION STATEMENT (of this Report)

Approved for public release; distribution unlimited.

17. DISTRIBUTION STATEMENT (of the abstract entered in Block 20, if different from Report)

18. SUPPLEMENTARY NOTES

19. KEY WORDS (Continue on reverse side if necessary and identify by block number)

turbulent flow
electric discharge laser
sub-ambient pressure

20. ABSTRACT (Continue on reverse side if necessary and identify by block number)

This work deals with the effect of reduced pressure in a controlled turbulent flow on electric discharge stabilization. A converging-diverging nozzle was designed and fabricated to provide a device for investigating this phenomenon. Turbulence was generated by perforated plates designed with a geometry that had proven to be successful in previous controlled turbulent

DD FORM 1473 EDITION OF 1 NOV 68 IS OBSOLETE
1 JAN 73
(Page 1) S/N 0102-014-6601 |

20. Abstract (Cont'd)

work. Turbulence and discharge data are presented along with photographs of the discharge for no flow, laminar flow and turbulent flow.

Sub-Ambient Controlled Turbulence Effects
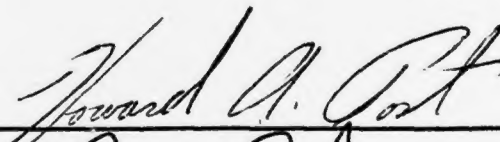on Discharge Stabilization for Laser Applications

by

Howard Allen Post
Lieutenant, United States Navy
B.S., Northrop Institute of Technology, 1967

Submitted in partial fulfillment of the
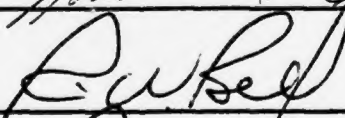requirements for the degree of

MASTER OF SCIENCE IN AERONAUTICAL ENGINEERING
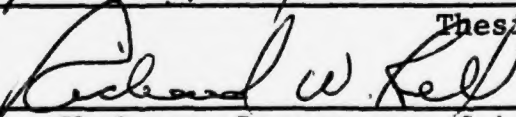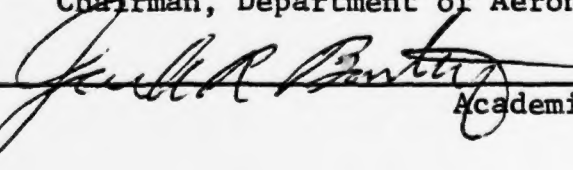
from the
NAVAL POSTGRADUATE SCHOOL
September 1976

Author	
Approved by:	for Oscar Biblarz
	Thesis Advisor
	Chairman, Department of Aeronautics
	Academic Dean

3

ABSTRACT

This work deals with the effect of reduced pressure
in a controlled turbulent flow on electric discharge
stabilization. A converging-diverging nozzle was designed
and fabricated to provide a device for investigating this
phenomenon. Turbulence was generated by perforated plates
designed with a geometry that had proven to be successful
in previous controlled turbulent work. Turbulence and
discharge data are presented along with photographs of
the discharge for no flow, laminar flow and turbulent flow.

4

TABLE OF CONTENTS

LIST OF ILLUSTRATIONS

Figure

Figure

ACKNOWLEDGEMENTS

The author gratefully acknowledges Associate Professor Oscar Biblarz for the encouragement and guidance he furnished during the course of this investigation. Further acknowledgements are extended to the technical staff of the Department of Aeronautics under R. Besel and T. Dunton, particularly to R. Ramaker for his assistance in the fabrication of equipment used in this study and to C. Gordon and J. Hammer for their assistance in calibration of diagnostic equipment. Finally, acknowledgements to my wife and children for their patience, understanding and encouragement.

I. INTRODUCTION

Several classes of electric discharge gas laser devices
are currently under investigation. (Ref. 1) A stagnant or
no flow device accomplishes heat removal and discharge
stabilization by diffusion to cavity walls. Maximum prac-
tical power capability for this class of lasers is approxi-
mately 500 watts (W) with a 10 meter (m) glass tube. Another
one incorporates gas flow for convective cooling and dis-
charge stabilization by diffusion to cavity walls. These
devices have a practical power capability of 5kW with a
7 m glass tube. A similar class, using convective cooling,
increases discharge stabilization by various pre-ionization
techniques with power capabilities greater than 10kW.

Recent work with turbulent flow for discharge stabiliza-
tion adds a fourth class of laser devices which have prom-
ising power capability. Biblarz and Nelson (Ref. 2) report
significant discharge power increases with ambient pressure
turbulent flow. Low pressure (80-200 Torr) turbulent flow
studied by Wiegand and Nighan (Ref. 3) found increased
discharge stabilization as a consequence of the turbulence.
Another low pressure study by Wasserstrom, Crispin,
Rom and Shwartz (Ref. 4) used a transverse secondary

9

flow to create vortical flow. They also found that vortex
flow had a significant effect on discharge stabilization.

The power capability of an electric discharge convec-
tive laser is scalable with mass flow rate (Ref. 5). The
mass flow rate can be increased by increasing density,
discharge area and velocity. Elevated pressure causes
difficulty with discharge stabilization but more power can
be coupled into the lasing mixture. No-flow breakdown
data at different discharge pressures for 4 cm and 8 cm
electrode gaps are presented by Loeb in Reference 6. Using
these data, breakdown power for increasing pressure is
shown in Figure 1. A single maximum is reached for a
given gap length, indicating an optimum discharge pressure.
The purpose of this project is to investigate the effect
of sub-ambient controlled turbulence flow on discharge
performance in the range above 450 Torr.

Section II deals with selecting an economically fabri-
cated device to explore the desired region and discusses
the general philosophy supporting its design. A complete
description of the entire apparatus is presented in Section
III. The experiment was divided into two primary areas,
turbulence tests and discharge tests, which are discussed
in Section IV. The results of the experiment and conclusions,
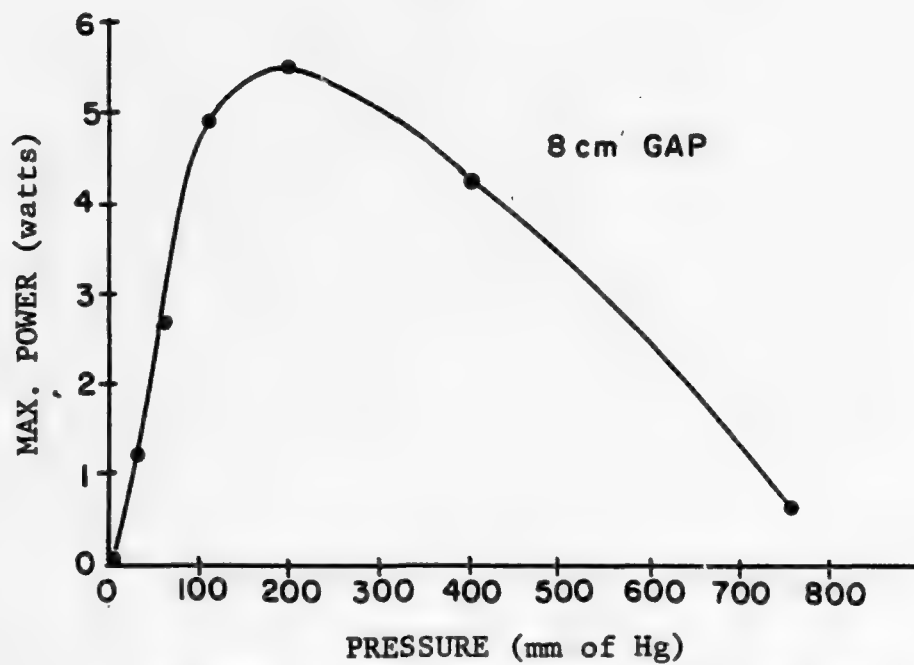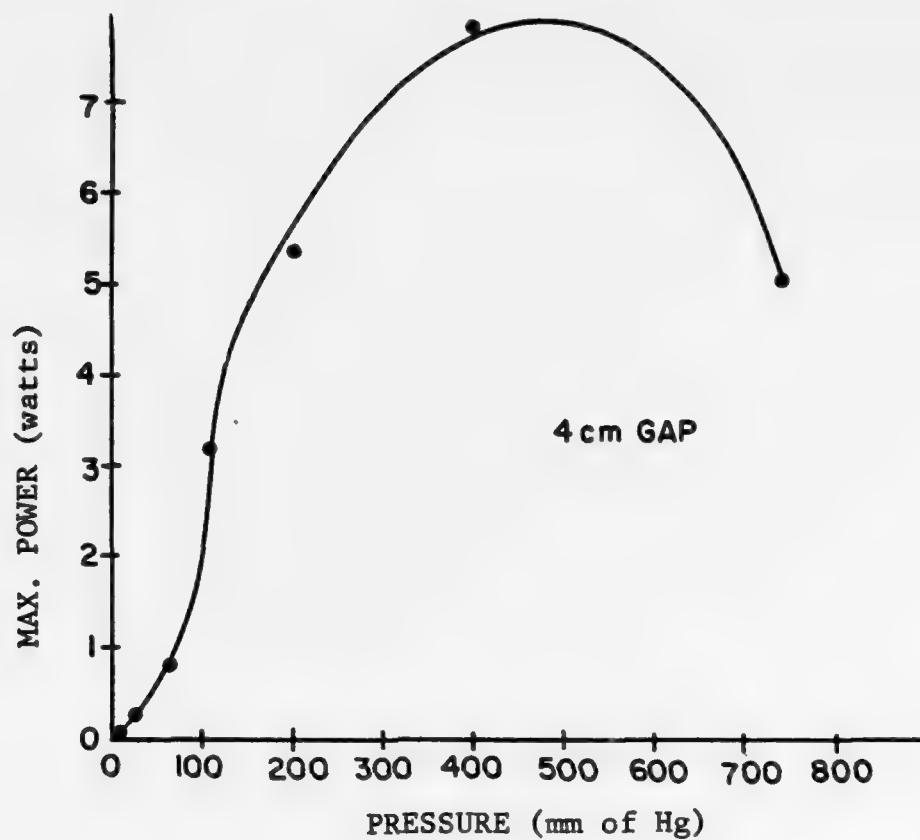
Figure 1. Breakdown Power Versus Pressure (Loeb Data, Ref. 6)

11

with some recommendations for improvement, are found in Sections V and VI respectively.

An interesting model of space charge convection effects is presented in Reference 7. Numerous experiments were conducted during this project to provide data to help establish and support the proposed model. Air was used for the discharge medium in all tests performed during this project. A CO_2, N_2 and He mixture would be expected to produce superior results.

II. REDUCED PRESSURE SYSTEM DESIGN CRITERIA

The design for reducing pressure in the electric dis-
charge test section resulted from a preliminary study of
two gasdynamic methods. First, the possibility of using
a converging nozzle, such that the inlet was open to
atmospheric air and the exit coupled to an evacuated
reservoir, was considered. A pressure ratio of sixty per
cent of atmospheric air could be obtained in the test
section. However, the flow rate required to produce
this pressure reduction combined with the need for at
least a two minute run time dictated the use of a reservoir
and vacuum pump much larger than was locally available.
This approach, therefore, was subsequently abandoned.

An alternative method which consists of using the flow
characteristics of a converging-diverging nozzle was adopted.
The system is driven by compressed air at the inlet, with
the diffuser exit open to atmospheric air. A short, con-
stant area section at the throat of the nozzle houses the
electrodes for the electric discharge test section. The
turbulence generating plates used in the experiment present
approximately fifty per cent area blockage to the flow.
To avoid choking the flow at the plate prior to reaching

13

desired test section conditions, a plate chamber was located upstream of the test section in the converging portion of the nozzle.

The specific design of the nozzle was based on three required features. First, a pressure ratio of sixty per cent of atmospheric air and Mach 0.95 were the desired maximum operating conditions in the test section. Test section conditions would be reached when flow through the plate chamber, which housed a plate with fifty per cent area blockage, reaches Mach 0.3. The section linking the plate chamber with the test section had to be as short as possible, thereby keeping the turbulence generating plate within reasonable range of the test section. With this configuration discharge density would be a function of velocity but it was concluded that the effect of these two parameters on discharge stability could be separated. Details of the various sections are presented in Section III.

It is known that vortex stretching occurs in accelerated flow of a wind-tunnel contraction, thus attenuating the low frequency, high energy turbulent spectrum of the flow. (Ref. 8) The location of the turbulence generating plate inherently placed the produced turbulent flow in this adverse environment. Low frequency, high energy turbulence is known to have a stabilizing effect on the discharge. (Ref. 2)

14

It was felt that the plate hole dimensions could be altered to compensate for the attenuation and that the plate was located close enough to the test section to insure adequate turbulent flow through the discharge. This was later found to be incorrect. Turbulence decay was measured and is discussed in Section V.

Since breakdown conditions are slightly variable with changes in water vapor partial pressure (Ref. 9), a study was conducted to determine a method for drying the air supply. Chemical dryers provide the most effective means for drying moist air but commercial products capable of accommodating the expected flow rates are large, expensive units thus precluding their use. To provide consistency of measured data, the effect of relative humidity had to be taken into account. It was decided that breakdown voltage data would be corrected to a standard humidity of 0.6085 inches of mercury vapor pressure by applying a correction factor determined from curves presented in Reference 9. The procedure used for determining the partial pressure of water vapor in the discharge region, and the correction factor curve, are presented in Appendix A. Recent work related to water vapor effects on breakdown voltage can be found in Reference 10.

III. EXPERIMENTAL APPARATUS

The experimental apparatus is composed of three major subsystems. These subsystems include an air flow system, a variable high-voltage D.C. discharge circuit, and a turbulence measurement system. Figure 2 is a photograph of the laboratory and most of the equipment used in the experiment.

A. THE FLOW SYSTEM

The flow system consists of an air compressor, water-cooler heat exchanger, flow rate control valves, a plenum section and a converging-diverging nozzle. Figure 3 is a schematic of the entire flow system. Air supply is provided by a Carrier three-stage centrifugal compressor with a 4000 ft^3/min. capability at a maximum pressure of two atmospheres. The flow is directed through a water-cooler heat exchanger that maintains a stabilized flow temperature at approximately 90°F.

Three gate valves are used to control the flow rate through the test section. Two of these valves are located downstream of the heat exchanger and are the primary control valves for the flow. It was determined that the flow choked in the heat exchange when the primary valves were set for

16

Figure 2. Laboratory Equipment
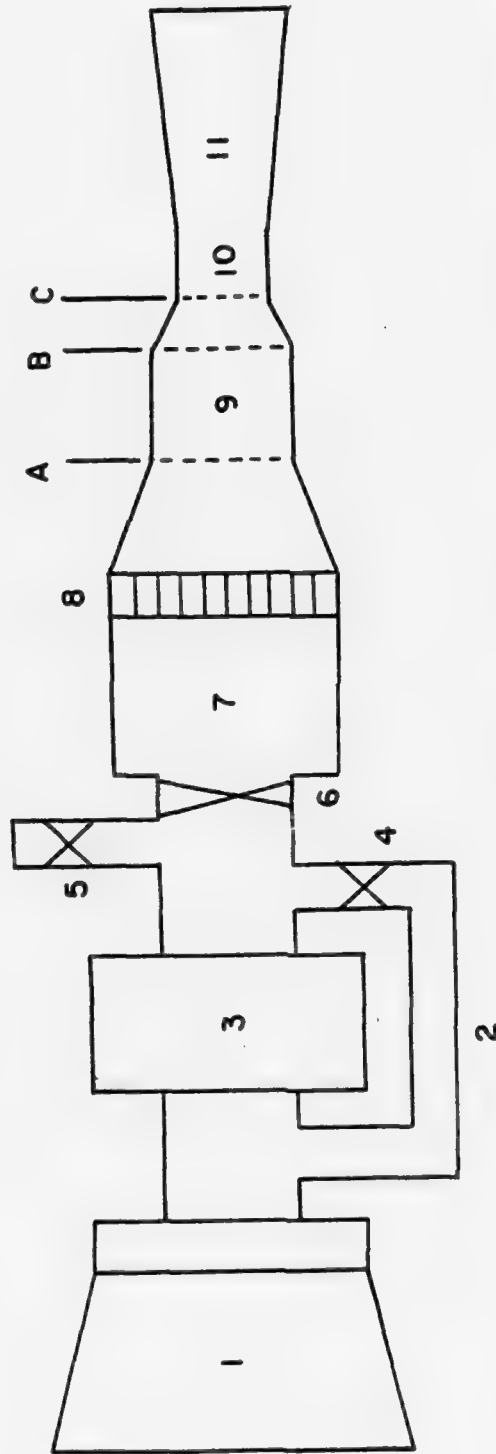
1. Compressor
2. Heat Exchange By-Pass
3. Heat Exchanger
4. Gate Valve
5. Gate Valve
6. Gate Valve
7. Plenum
8. Honeycomb
9. Plate Chamber
10. Test Section
11. Diffuser

NOTE: A, B, and C are locations discussed in the text.

Figure 3. Flow System Schematic

maximum flow and this, therefore, necessitated the installation of a heat exchanger by-pass controlled by the third gate valve. The by-pass eliminates the problem and full flow is available.

A plexiglass plenum chamber used in Reference 11 was incorporated into this apparatus but it catastrophically failed during early operation and was subsequently replaced with a 3/4 in. thick, plywood structure. The plywood plenum joints were glued and reinforced. Internal and external surfaces were sealed to prevent moisture absorption. Aluminum honeycomb inserts dampen upstream turbulence and straighten the flow in the plenum.

The converging-diverging nozzle is a plexiglass assembly of five individual sections. The assembled nozzle is shown in Figure 4. A converging section connects the original plexiglass plenum chamber to the plate chamber. The inside dimensions for the inlet, i.e., 9 in. x 9 in. were selected to integrate the new nozzle with the structure already present. The inside dimensions of the exit match that of the plate chamber.

A plate chamber houses and supports the turbulence generating plates. The chamber's cross sectional area of 20 in.^{2} was selected so that at maximum operating conditions, i.e., Mach 0.3 flow in the plate section, the corresponding
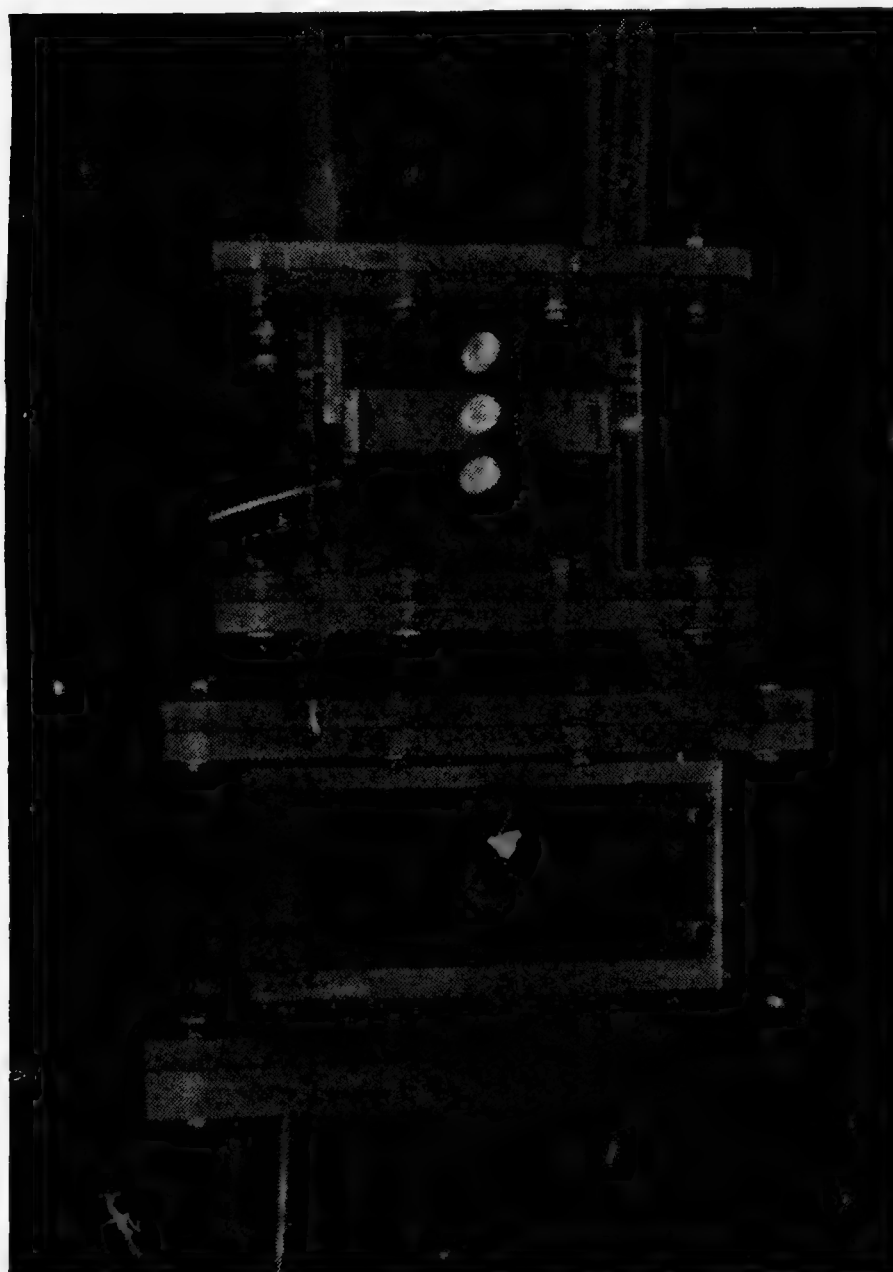
Figure 4.   Nozzle Assembly

test section area (based on isentropic relations, Ref. 12) would be of sufficient size to house the electrodes. Removal of a pressure tight hatch allows easy access to the plate which, therefore, can be readily changed. The plate chamber is schematically illustrated in Figure 5.

A short converging section links the plate chamber with the test section. Its length was determined by fabrication factors and the desire to have the plate as close as possible to the test section. The test section provides support for the electrodes and includes a number of features. The cathode can be moved to provide various electrode spacings, with a minimum spacing of 2.9 cm. Numerous threaded ports in the walls of the test section provide access for diagnostic probes which are secured in position by pressure tight fittings. The test section schematic is presented in Figure 6. A photograph of the fabricated section is shown in Figure 7.

The diffuser section has an overall length of 41.18 inches and a wall divergence angle of 2.5 degrees. Tufts were placed along the diffuser wall to check visually for flow separation.
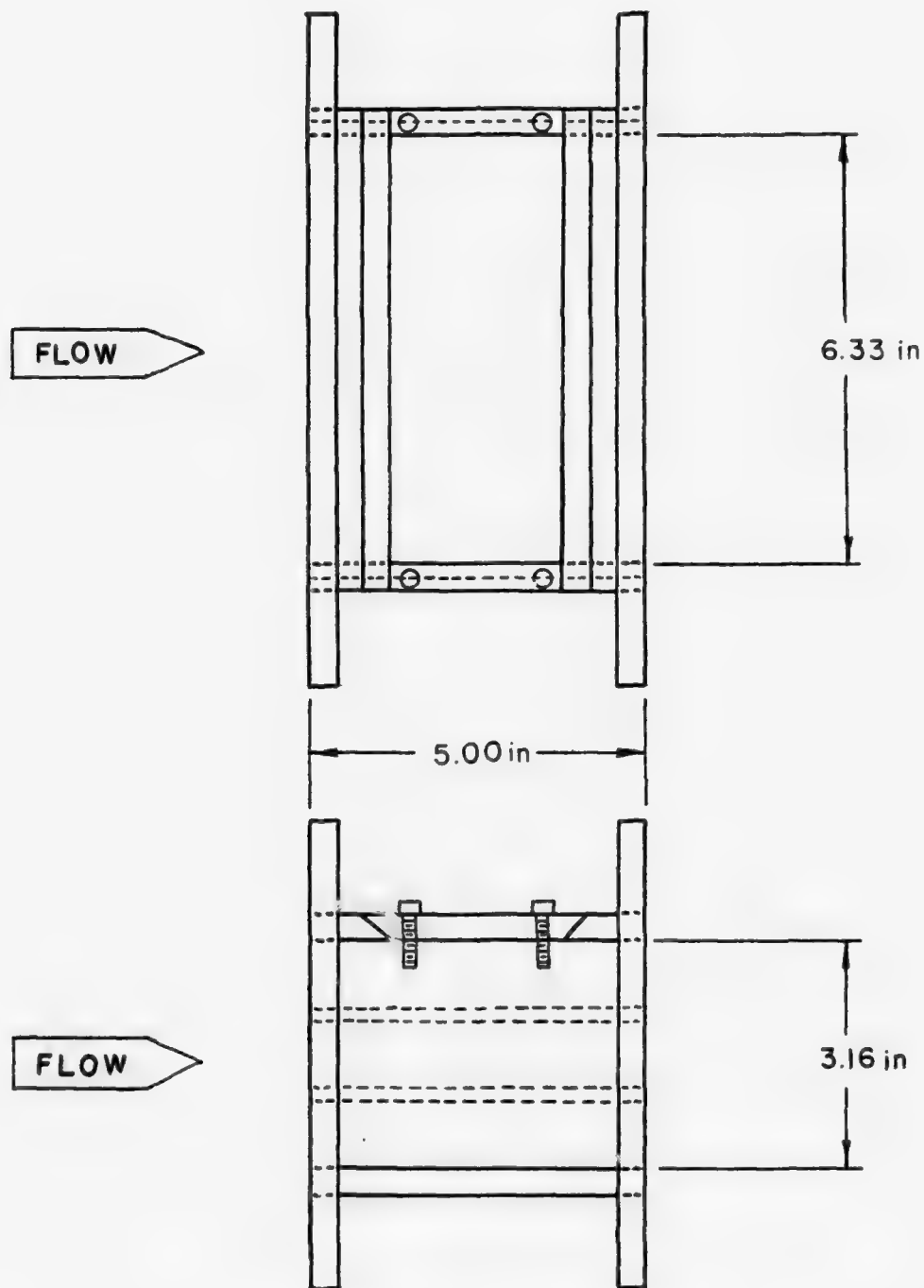
MATERIAL: 0.75 INCH PLEXIGLASS

Figure 5.   Plate Chamber Schematic
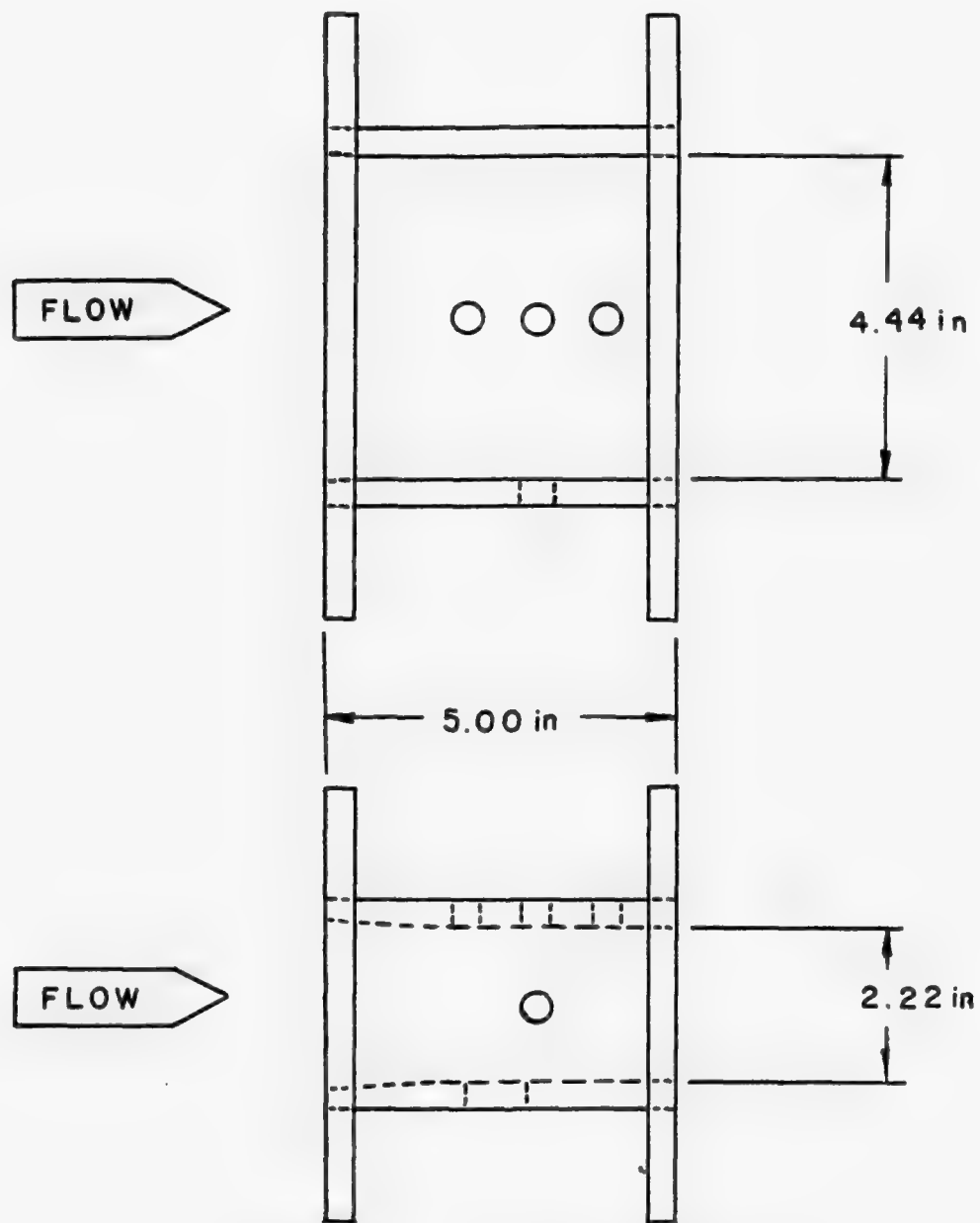
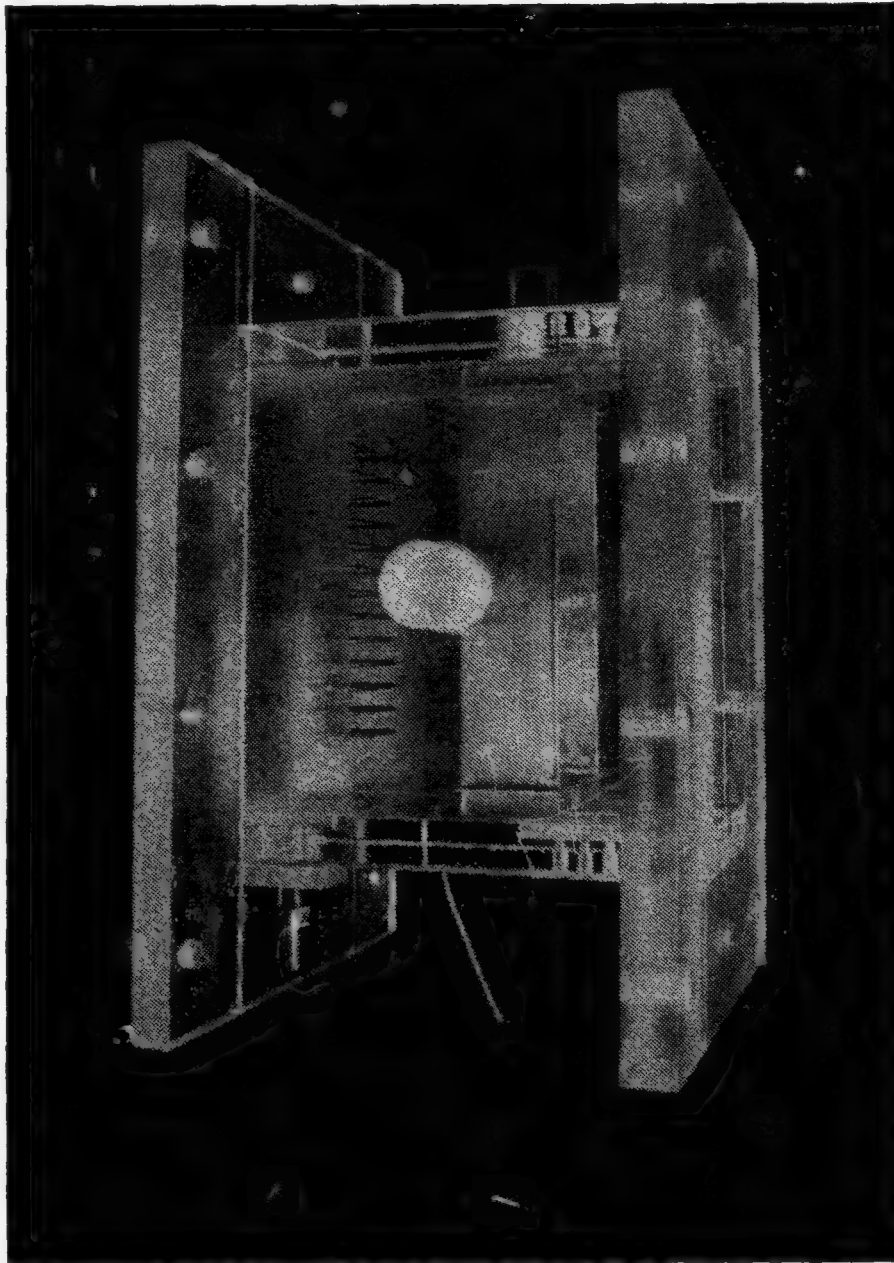MATERIAL: 0.75 INCH PLEXIGLASS

Figure 6. Test Section Schematic

FLOW ⇒

Figure 7.   Test Section

24

B. THE DISCHARGE CIRCUIT

Three primary elements comprised the variable voltage, D.C. discharge circuit. These elements include a variable high-voltage, D.C. source, the discharge electrodes and current/voltage meters. Figure 8 is a schematic of the circuit.

Two high-voltage power supplies were available and were independently used in the experiment. A Sorenson high-voltage, D.C. power supply with a maximum output of 30 kilovolts (kV) and 20 milliamperes (mA) powered the electric discharge in most of the tests. An old Sorenson Beta high-voltage, D.C. power supply with a rated maximum output of 60kV and 50mA was also used but found capable of producing only 34kV and 18mA. The power supplies were interchanged to cross check measurements of experimental discharge power data. Excellent agreement was observed.

The discharge electrodes consist of a pin anode arrange-ment similar to Aunchman's (Ref. 11) and a wire grid cathode. The anode pins were made from 0.0625 inch steel wire and mounted on an airfoil machined from 0.5 to 0.125 inch brass strip. Figure 9 shows the details of the pin electrode. The wire grid cathode arrangement resulted from a series of preliminary tests utilizing Aunchman's equipment. The airfoil cathode used by Aunchman was replaced by an aluminum
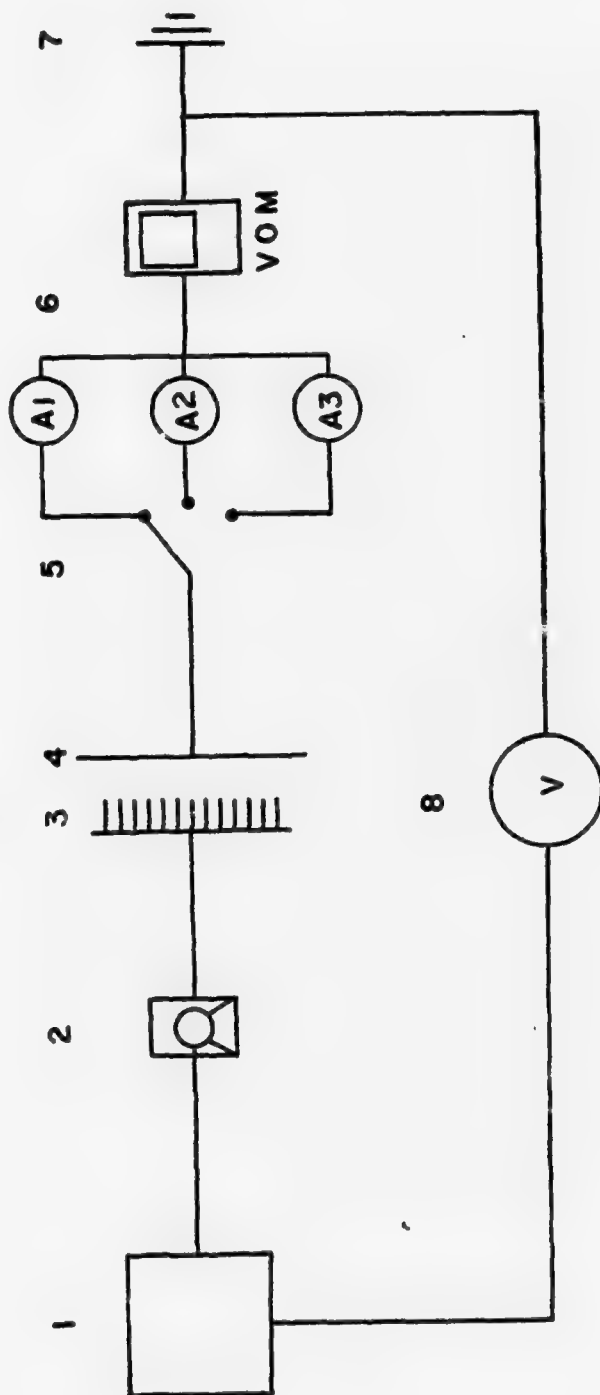
1. Power Supply
2. Oil Submerged Brass Sphere
3. Pin Anode
4. Wire Grid Cathode

5. "Make-Before-Break" Switch
6. Ammeters
7. Laboratory Ground
8. Voltmeter

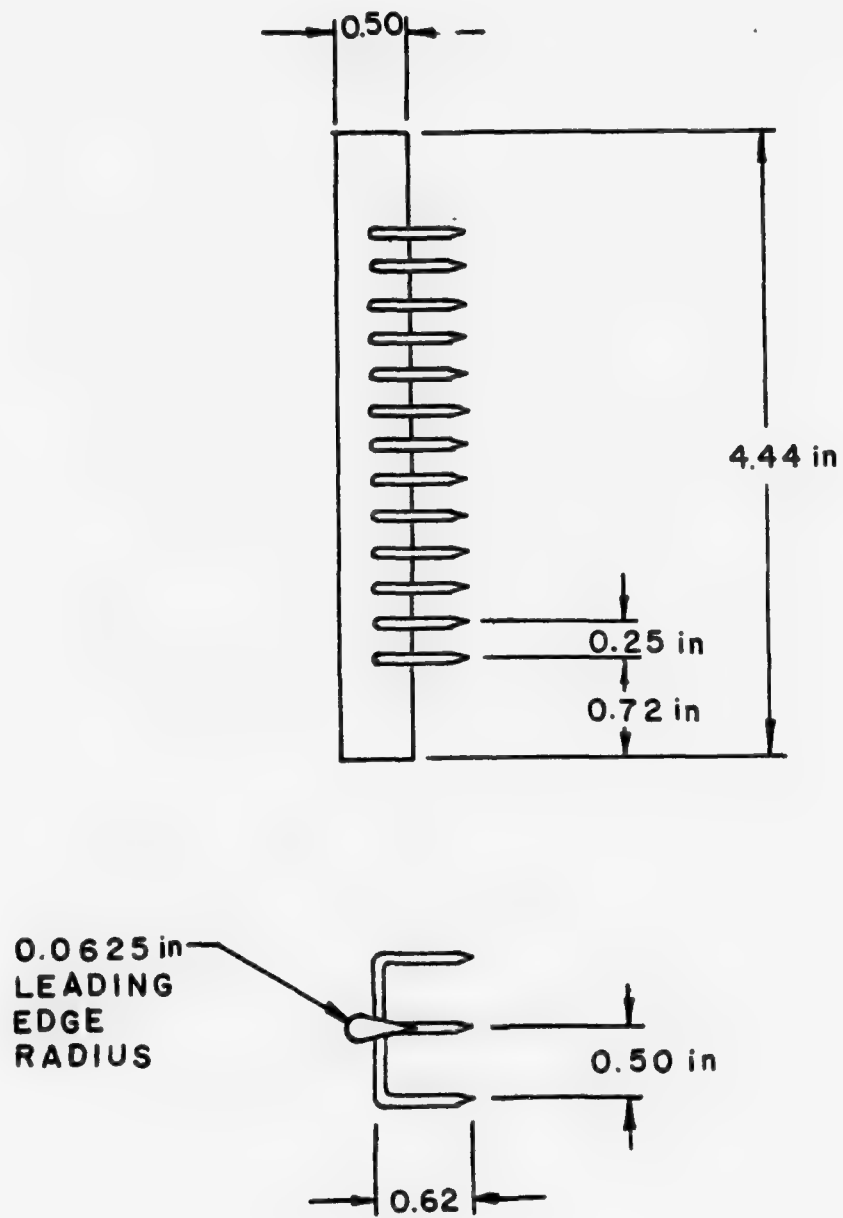Figure 8. High Voltage Discharge Circuit

Figure 9.   Pin Anode Schematic

honeycomb cathode to establish a more uniform field, and did perform slightly better than the airfoil arrangement. The honeycomb cathode was not rigid enough to withstand the flow forces and hence was replaced by a wire grid cathode which performed just as well. It was learned later that wire grid cathodes are the preferred cathode geometries of axial flow systems. (Ref. 13) A photograph of the electrodes is shown in Figure 10. Mounted on the pin anode is plate III used in the tests and described later.

Current measurements were taken with three Triplett milliammeters with ranges from 0.0 to 1.0, 10.0 and 50.0 milliamperes wired in series through a "make before break" switch. A Simpson 260 V-O-M was also used for a cross check measurement of current. Originally, discharge voltage was measured with a Sensitive Research electrostatic voltmeter but a short circuit was detected in the meter and precluded its use. The power supply control panel voltmeter readings are within one per cent of the Sensitive Research meter and it was therefore used to measure the discharge voltage. This error was taken into account when an error bar for measured breakdown voltage was determined. High-voltage leads were used throughout the circuit. Power supply connections were made through a highly polished, oil submerged, brass sphere.
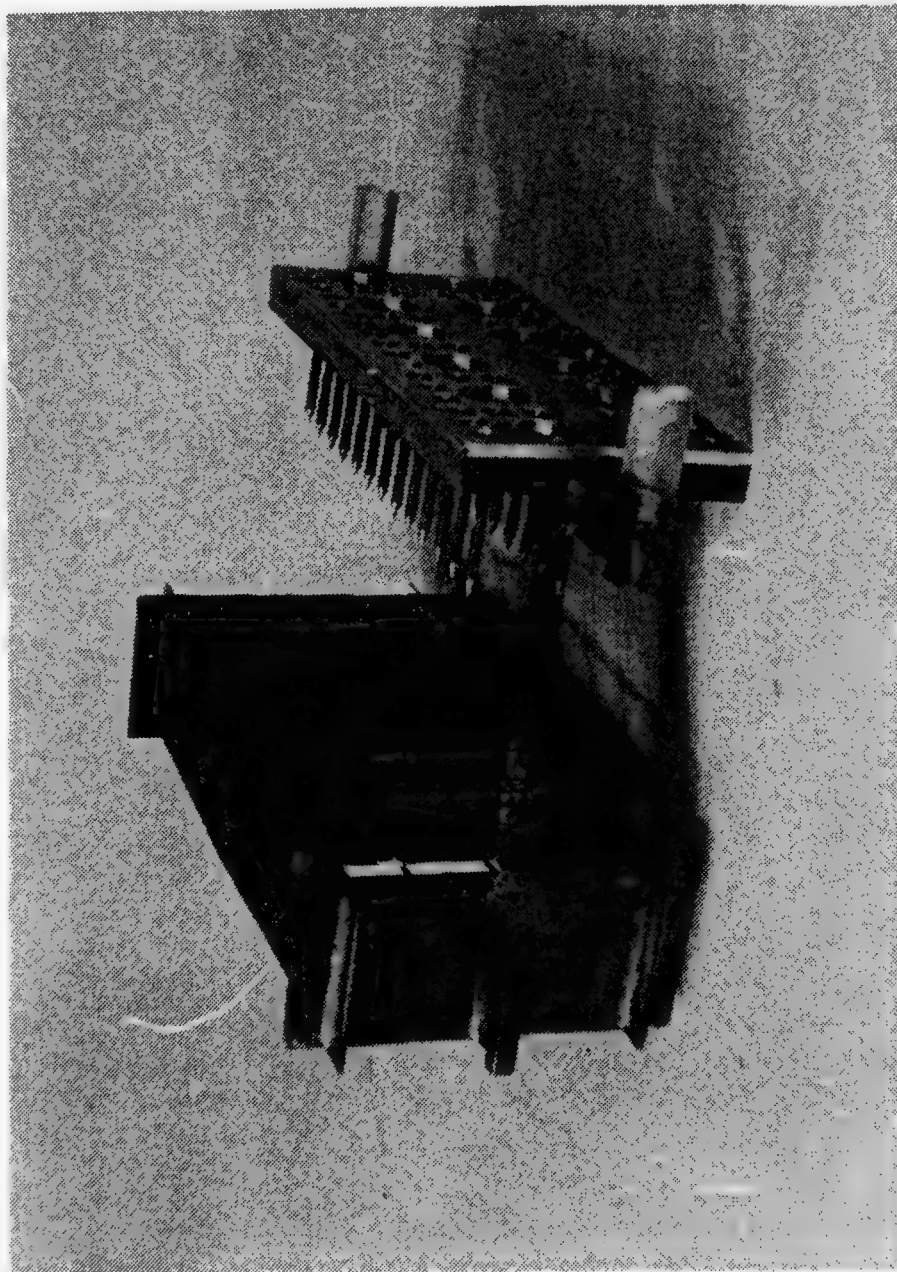
Figure 10. Electrodes

C. TURBULENCE EQUIPMENT

Turbulence diagnostic equipment includes a Thermo Systems Inc. hot wire anemometer, a Hewlett-Packard oscilloscope, a General Radio Company, Type 1921, real time analyzer and a Hewlett-Packard 7035B X-Y recorder. Hot wire probe filaments are 0.00015 inch diameter tungsten wires spot welded to the probe supporting pins. Hot wire anemometer components include a model 1051-2 monitor and power supply and a model 1054A-20 anemometer module.

The oscilloscope was used for setting and adjusting the stability and frequency response of the anemometer. Difficulty was encountered in matching probe/anemometer impedance following the procedure outlined in the operators manual. To alleviate the problem, various lengths of coaxial cables were kept on hand for coarse impedance matching, followed by fine adjustments of the anemometer. In general, the hot-wire system proved difficult to use. Considerable skill and time were required to spot weld the tungsten wires in place. The wired probes were fragile and required frequent replacement.

The real time analyzer is composed of a model 1925, 30 channel multifilter and a model 1926 multichannel RMS detector. Based on experience gained in Reference 2,

30

four-second integration times were used during all measure-
ments. The X-Y recorder enables rapid and accurate data
collection from the memory output of the analyzer. All
equipment is grounded through a separate grounding system
in the laboratory.

D. OTHER DIAGNOSTIC EQUIPMENT

A number of diagnostic instruments used in the experi-
ment were fabricated locally. Iron-constantan and copper-
constantan thermocouples were used for total temperature
measurements. A pitot-static probe, using either water
or mercury manometers, provided pressure data. The thermo-
couples and pitot-static probe were carefully calibrated
at a local facility. Pressure and temperature measurements
of a free jet from Mach 0 to Mach 1.0 were compared with
highly accurate reference probes. The calibration pro-
cedure resulted in detection of a faulty probe, which was
discarded, and permitted a high level of confidence in
experimental measurements. Other diagnostic equipment was
also calibrated according to operating manuals. Calibra-
tion results were used to estimate an error bar for the
various measured test parameters. Error analysis is
presented in Appendix B.

IV. EXPERIMENTS CONDUCTED

The experiments performed were divided into two main
areas. First, turbulence spectrum sampling was required to
investigate the amount of turbulence decay encountered with
accelerated flow in this apparatus and to make necessary
modifications. Large eddies must be present in the dis-
charge region to have a stabilizing effect in breakdown
as evidenced by Reference 1 and Reference 4. Second, maxi-
mum discharge performance was to be investigated with
turbulent and non-turbulent flow. The diffuser was removed
to obtain reference data at near atmospheric conditions.
With the diffuser on, density reduction effects could then
be studied.

A. TURBULENCE TESTS

In Reference 11, spectrum distributions were obtained
for various plates. Plate 9 had produced the most intense,
homogeneous turbulence distribution. However, discharge
performance tests at a velocity of 200 ft/sec. (61 m/sec.)
showed Plate 1-6 outperformed Plate 9. Preliminary tests
using these plates and Aunchman's test section, showed
that Plate 9 was superior at higher velocities. Plate 9

geometry was adopted for use in the current apparatus.
The various plate modifications used are identified as
Plates I, II and III. Figure 11 describes these plates
in detail.

A spectrum distribution of the turbulence generated
by the pin anode was recorded at a test section velocity
of 200 ft/sec. (61 m/sec.). Plate I was used to investi-
gate spectral decay associated with flow acceleration.
This was accomplished by placing Plate I at the upstream
end of the plate chamber. (Position A, Fig. 3). Turbulence
spectrum was measured in the chamber 3.5 inches (8.89 cm)
downstream of the plate. Plate I was then relocated at
the downstream end of the chamber (Position B, Fig. 3) and
turbulence in the test section 3.5 inches (8.89 cm) down-
stream of the plate was recorded. Comparing the spectra
obtained by this procedure, acceleration effects on turbu-
lence were determined. Spectrum decay was much greater
than initially anticipated. Plate II was manufactured and
tested in the same manner. With Plate II installed at
location B, spectra in the test section were measured with
and without the diffuser.
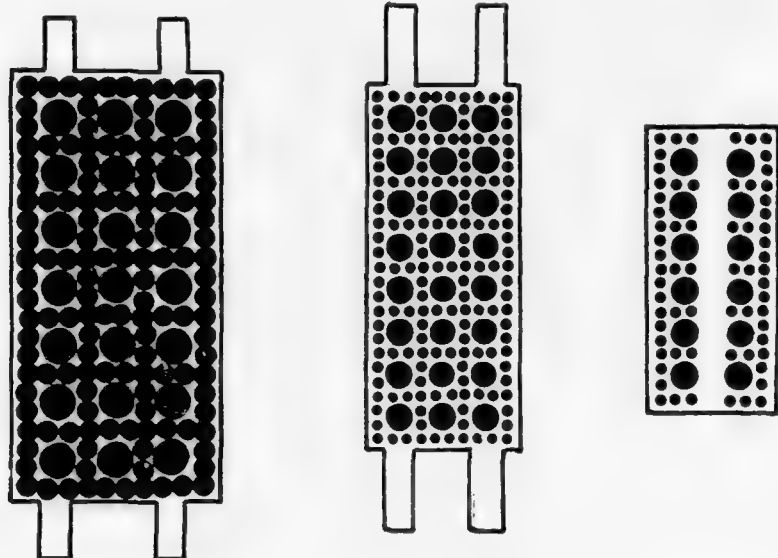
	I	II	III
	Plate I	Plate II	Plate III
	I	II	III
MATERIAL:	COPPER	PHENOLIC	ALUMINUM LAMINATED ON PHENOLIC
LENGTH (IN.)	6.0	5.2	3.6
WIDTH (IN.)	2.6	2.2	1.5
THICKNESS (IN.)	0.125	0.18	0.25
DIAMETER (IN.)			
LARGE HOLES:	0.50	0.375	0.375
SMALL HOLES:	0.187	0.125	0.125

Figure 11.   Turbulence Generating Plates

34

B. DISCHARGE PERFORMANCE TESTS

This part of the experiment involved discharge power
performance under the influence of the various plate and
nozzle arrangements used in the turbulence tests. Three
internal configurations were studied with the diffuser
removed. First, maximum discharge performance with in-
creasing velocity was measured for a no-plate, "laminar"
condition. Again, maximum discharge performance with in-
creasing velocity was recorded with Plate II installed in
the plate chamber. Since power supply limitations were
reached prior to obtaining optimum desired test section
conditions, it was decided to manufacture Plate III and
mount it on the immediate upstream edge of the pin anode.
This configuration is shown in Figure 10 and the plate
position is identified with position C in Figure 3. It
was anticipated that the flow would choke at the plate
prior to optimum discharge conditions, but it was felt that
power supply limitations would be reached prior to choking.
Attempts were made to obtain a turbulence spectrum of Plate
III in the discharge region, but hot wire tungsten fila-
ments could not survive this intense turbulent flow even
at low velocities. All the above tests were repeated with
the diffuser on.

35

A number of other tests involving variable voltage
rates and various gap lengths were performed to provide
a data basis for a model presented in Reference 7.

V. DISCUSSION OF RESULTS

Spectral data indicate that a severe low frequency
turbulence decay occurs for plates positioned at location
B (Fig. 3) in the accelerated flow. These data are pre-
sented in Figure 12. Comparing the unaccelerated spectrum
with the accelerated spectrum of Plate I illustrates the
decay encountered. Spectra shifted slightly to the right
with increasing velocity as was observed in Reference 11.
Plate III turbulence spectrum could not be measured, for
reasons previously stated, but some partial data did show
turbulence intensities above 40dB. No changes in the
spectrum were observed with diffuser on and diffuser off
nozzle configurations at a test section velocity of
200 ft/sec. (61 m/sec.).

Total mass flow rate through the nozzle was computed
from plate chamber diagnostics. Mass flow through the
discharge region was less than total mass flow because of
plate and pin anode blockage. The plate does not extend
from wall to wall. The width of the plate is less than
the total width of the test section and thus provides a
"boundary layer" slot. The slot allows higher mass flow
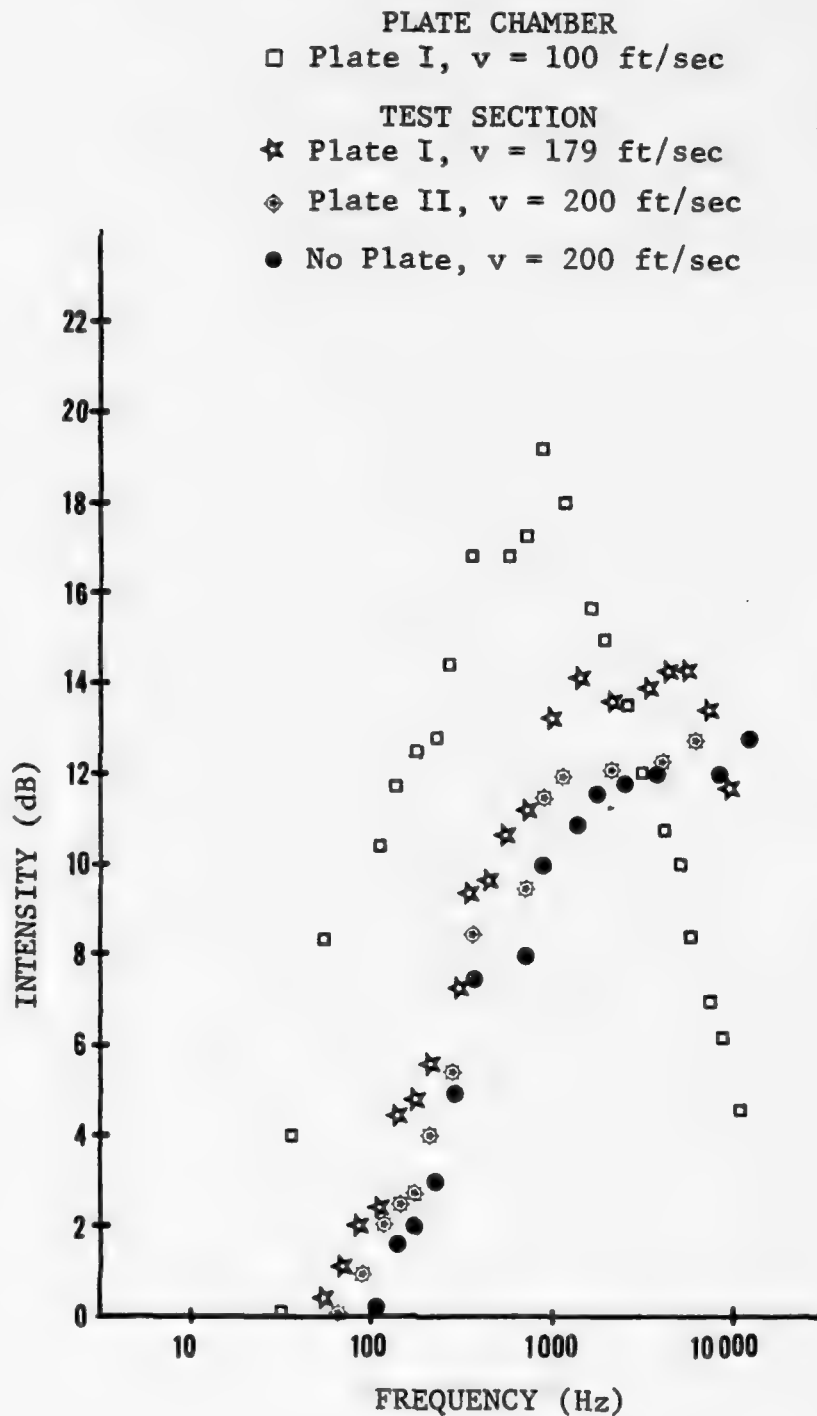along the walls to remove discharge waste heat and to

Figure 12.   Turbulence Spectra

remove any water condensation. Mass flow outside the discharge volume was determined from diagnostics in that region of the test section and subtracted from the total mass flow giving the mass flow rate through the discharge volume. Figure 13 was constructed from mass flow rate data.

An error analysis for discharge performance curves is presented in Appendix B. The magnitude of the computed error bar was extremely sensitive to pressure readings. At high pressures, mercury manometers were used producing a larger error bar than the readings from the water manometers.

Maximum discharge power per mass flow rate or energy per mass obtained for no plate "laminar" flow and turbulent flow using Plate III located at position C (Fig. 3) are presented in Figure 14. These curves show an initial decrease in energy per mass to a minimum and then rapidly increase. At low mass flow rates the total power remained relatively constant causing the initial decrease. As mass flow rate increased, convective cooling, turbulence and sub-ambient density increased the stability of the discharge resulting in greater total discharge power. The model presented in Reference 7 suggests how velocity,
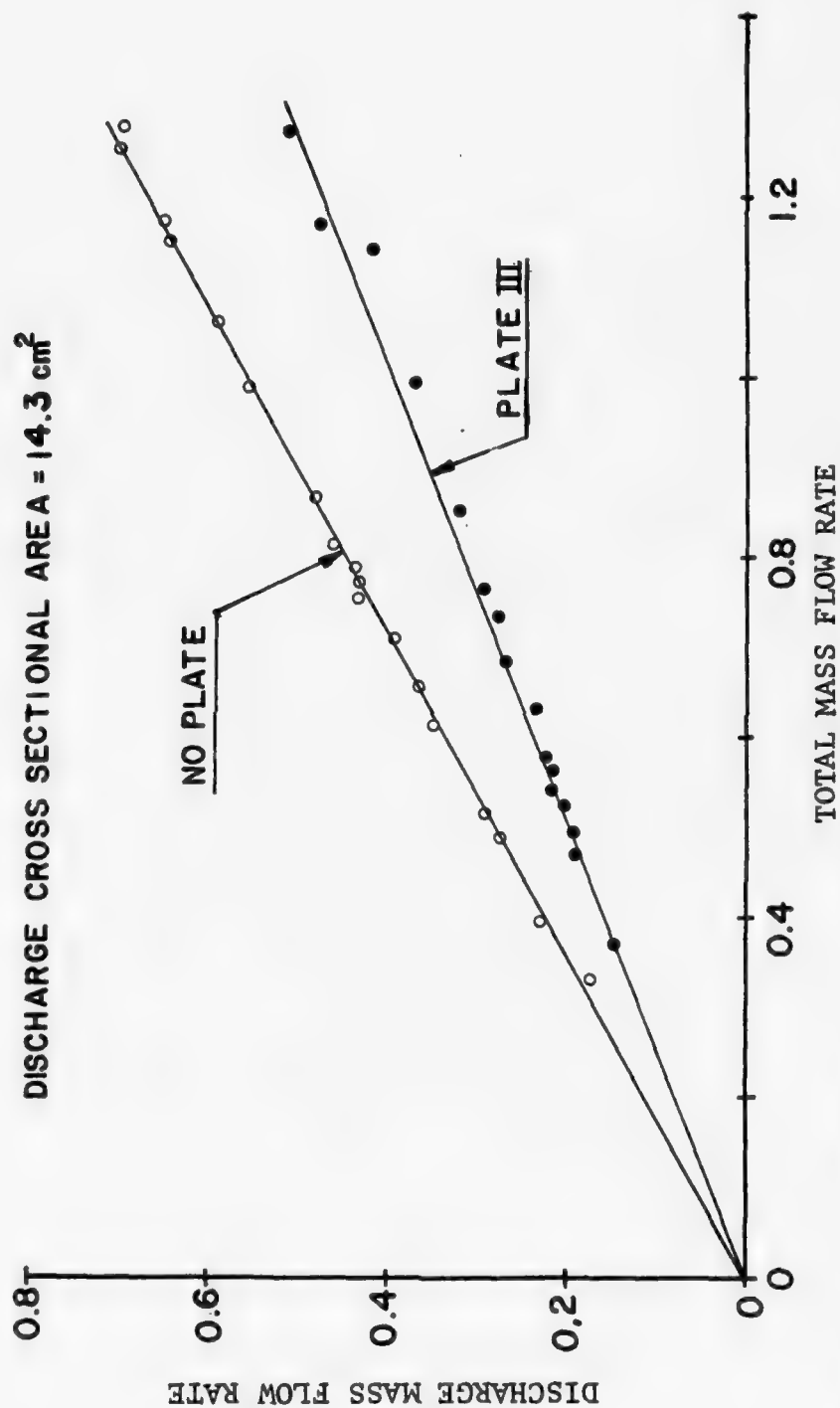
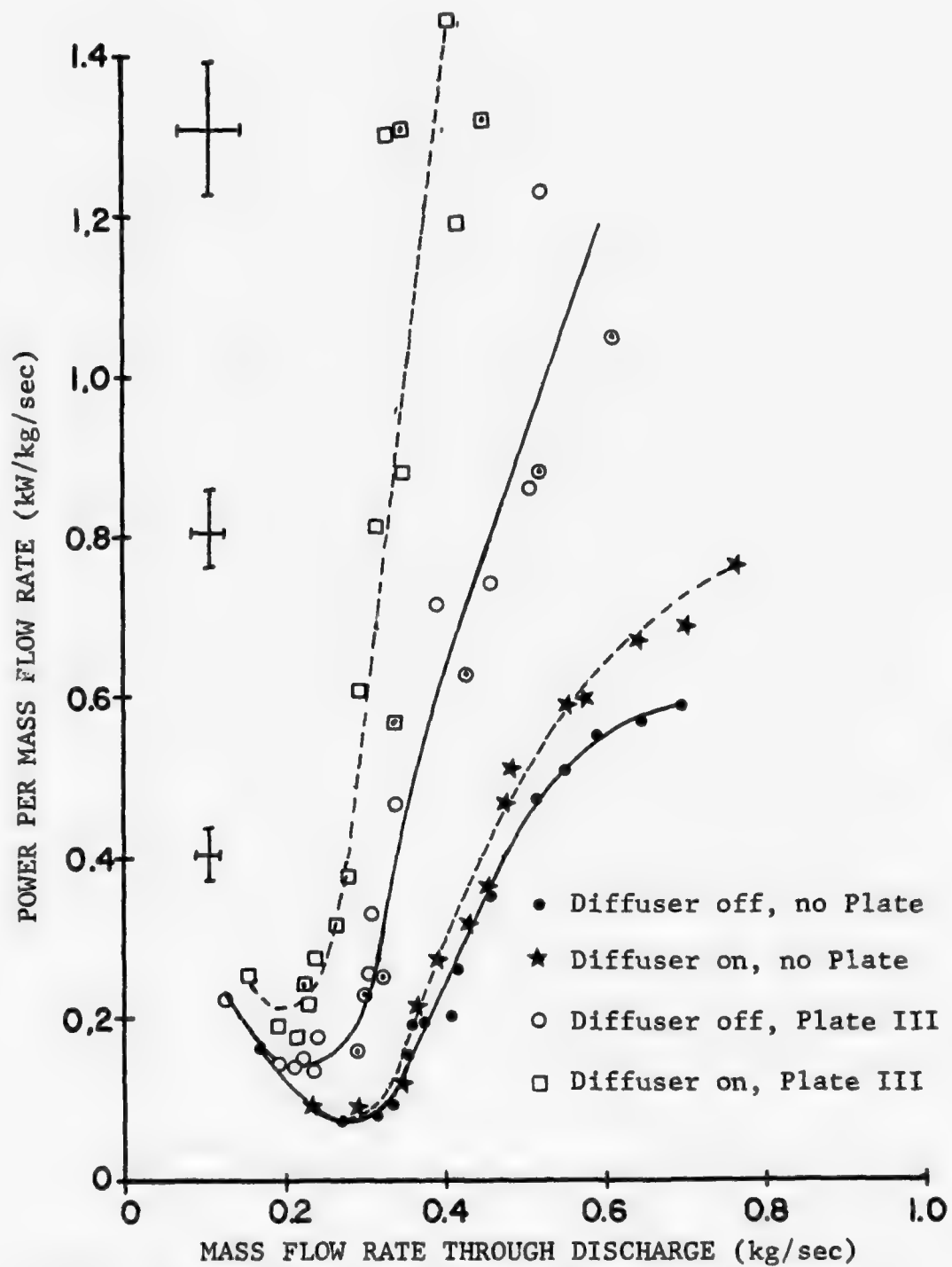Figure 13. Mass Flow Rate Through the Discharge Versus Total Mass Flow Rate

Figure 14. Power Per Mass Flow Rate Versus Mass Flow Rate Through the Discharge

41

turbulence and density influence discharge stability. The data presented here help support the validity of the proposed model.

Sub-ambient density effects on discharge stability caused an increase in energy per mass as was anticipated. The advantage of turbulent, sub-ambient flow can be realized from these curves. At the power supply current limited points, i.e., the last data point for each curve, more than twice the energy per unit mass was obtained for sub-ambient turbulent flow at about half the mass flow rate when compared with atmospheric "laminar" flow. Another way of looking at this is to superimpose lines of constant power on the curves of Figure 14 as shown in Figure 15. A given power level can be reached with sub-ambient turbulent flow at a much lower "cost" in mass flow rate.

Figure 14 also shows that the laminar curves appear to be approaching an upper bound on energy per unit mass while the turbulent curves are rapidly rising. Data from plates I and II were identical to the laminar curves, demonstrating the severe turbulence attenuation of the accelerated flow.
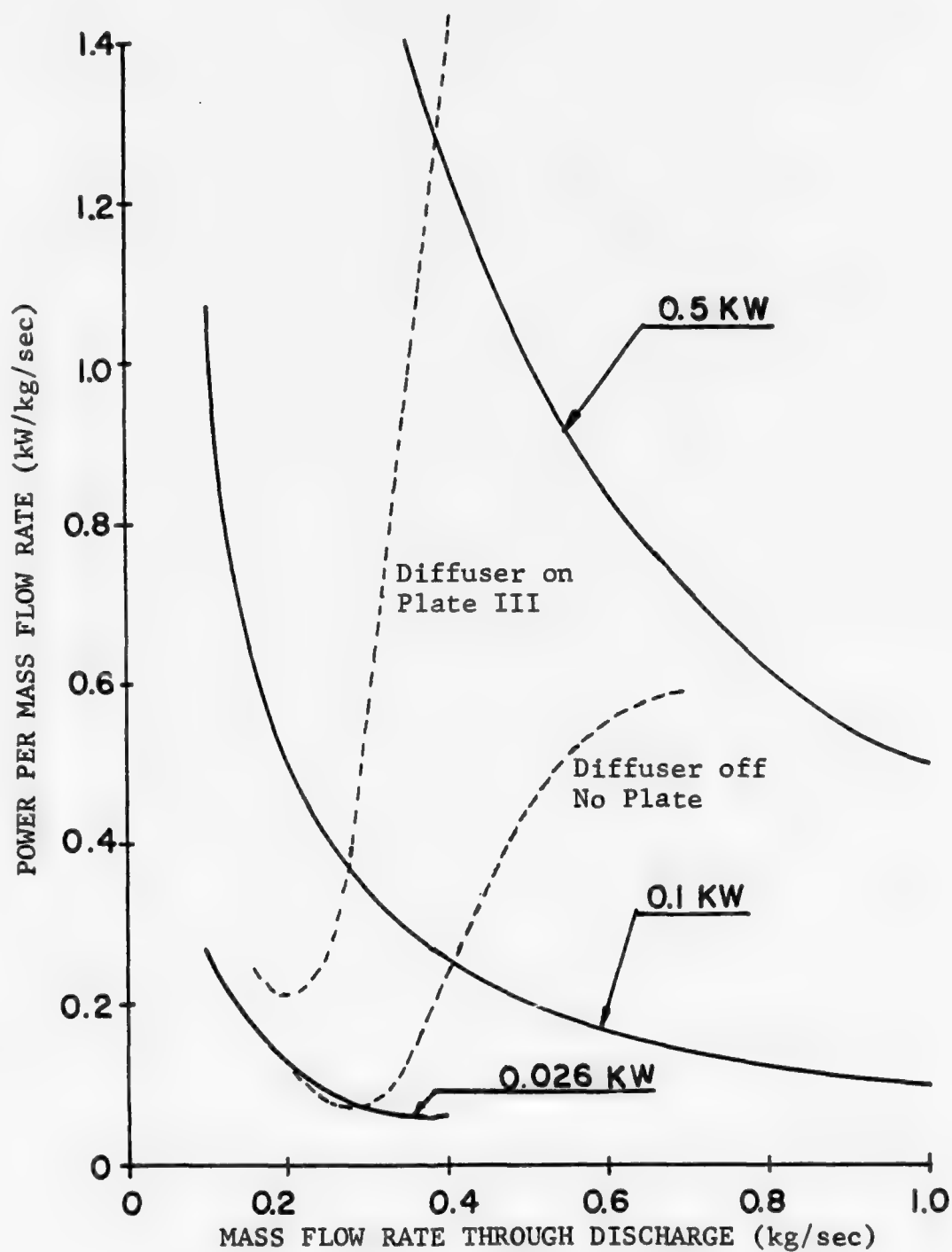
42

Figure 15. Constant Power Curves

43

An average discharge velocity was computed from discharge mass flow rates. Convective cooling and turbulent effects on discharge stability with increasing average discharge velocity can be seen in Figure 16. Increasing velocity provided convective cooling which increased discharge stability and hence greater power density. Higher power densities were obtained with turbulent flow at velocities greater than 60 m/sec. The slope of the "laminar" curve appears to be decreasing above 160 m/sec. Peak power would probably be reached at choked conditions. The extreme ends of the curves are power supply current limits, not energy density limits. Figures 17 and 18 give breakdown voltage and breakdown current data for increasing discharge velocity.

Photographs of the discharge near breakdown conditions taken for no-flow, "laminar" flow and turbulent flow are presented in Figure 19. The no-flow photograph was a ten-second exposure. The general appearance of the glow discharge shows a low intensity discharge extending between each pin and the cathode. The bright region at the bottom of the photograph resulted from a breakdown spark during the time exposure. In contrast, the "laminar" and turbulent flow photographs were one-second exposures. In
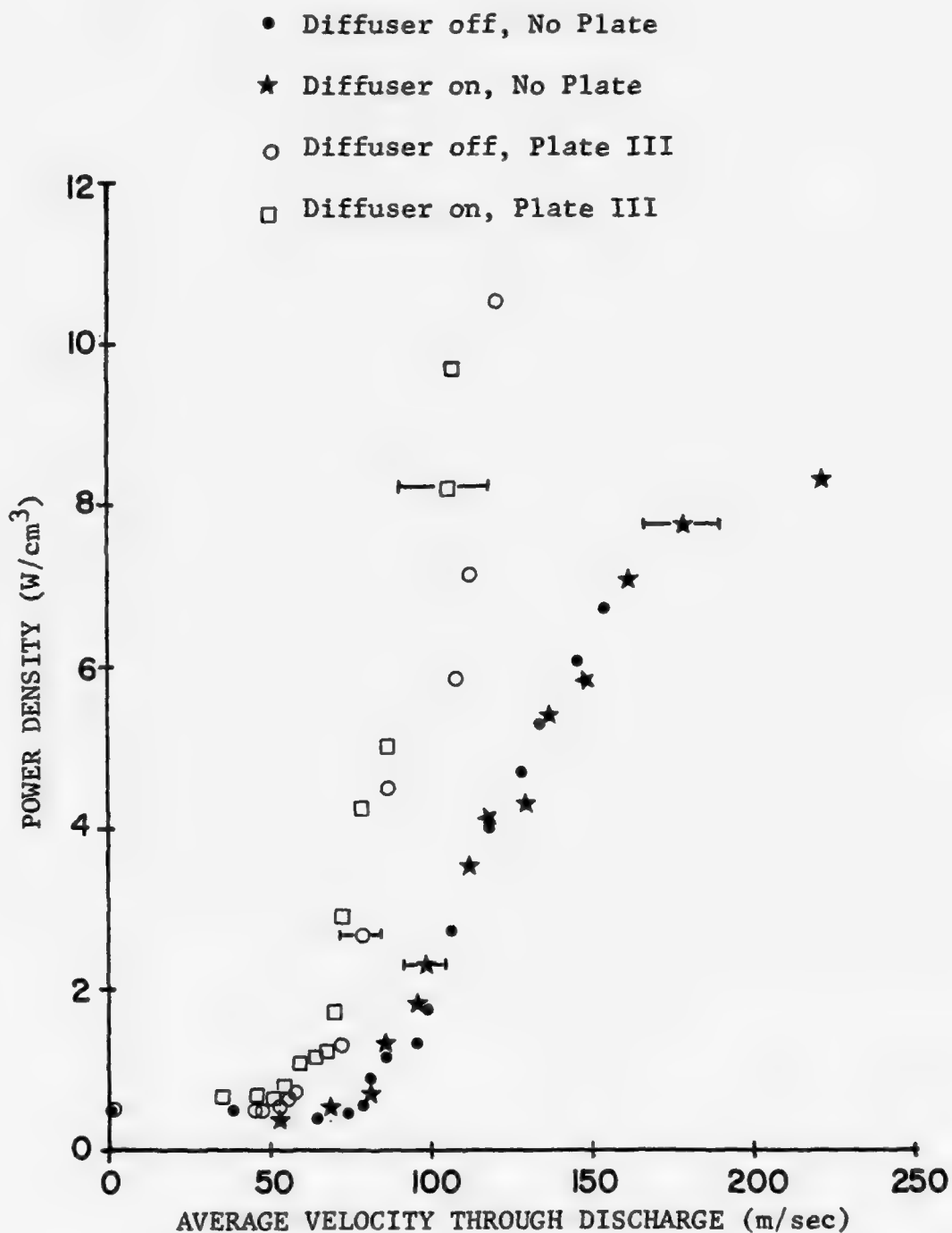
Figure 16.   Power Density Versus Average Velocity
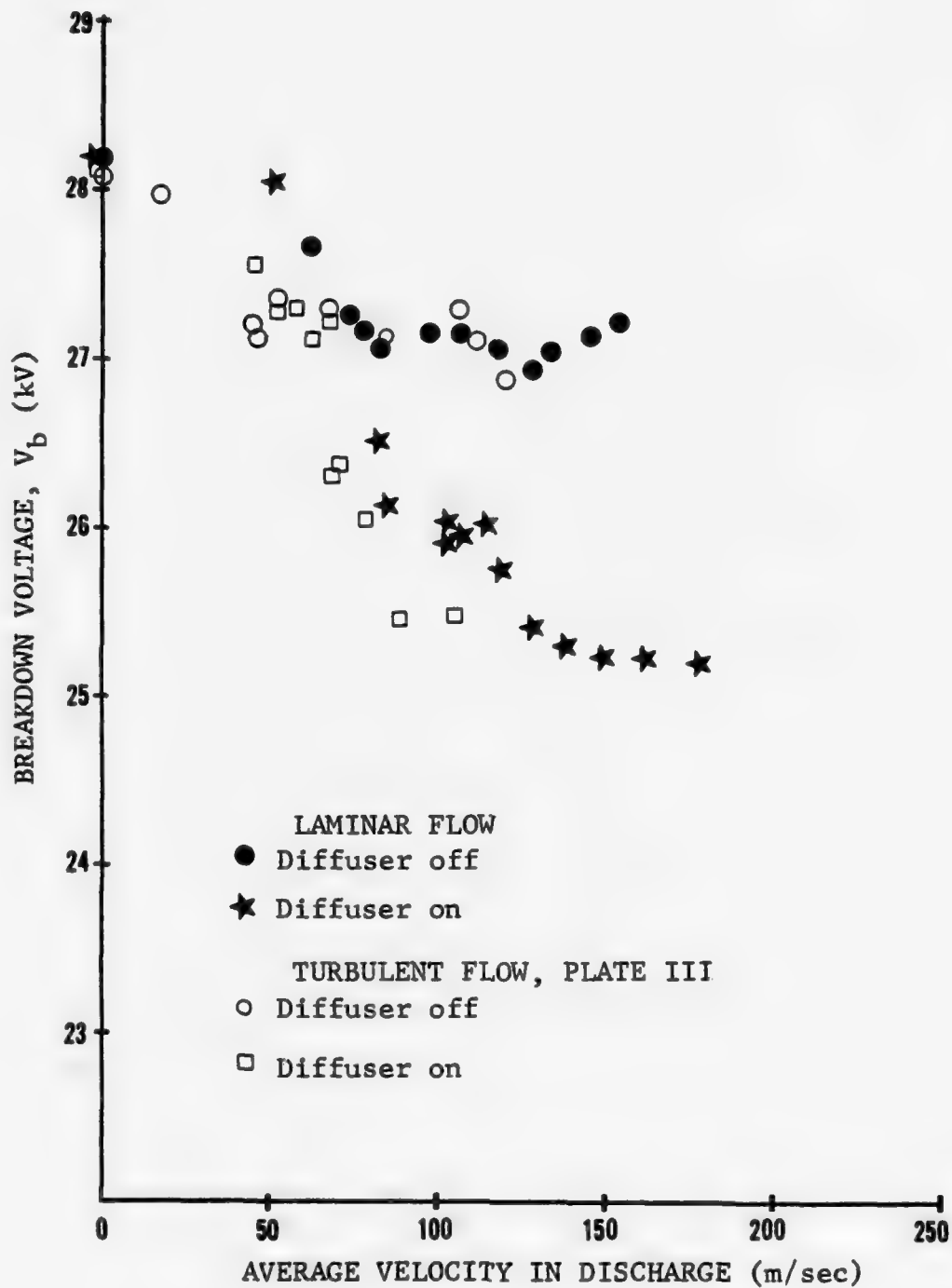Through the Discharge

Figure 17.   Breakdown Voltage Versus Average
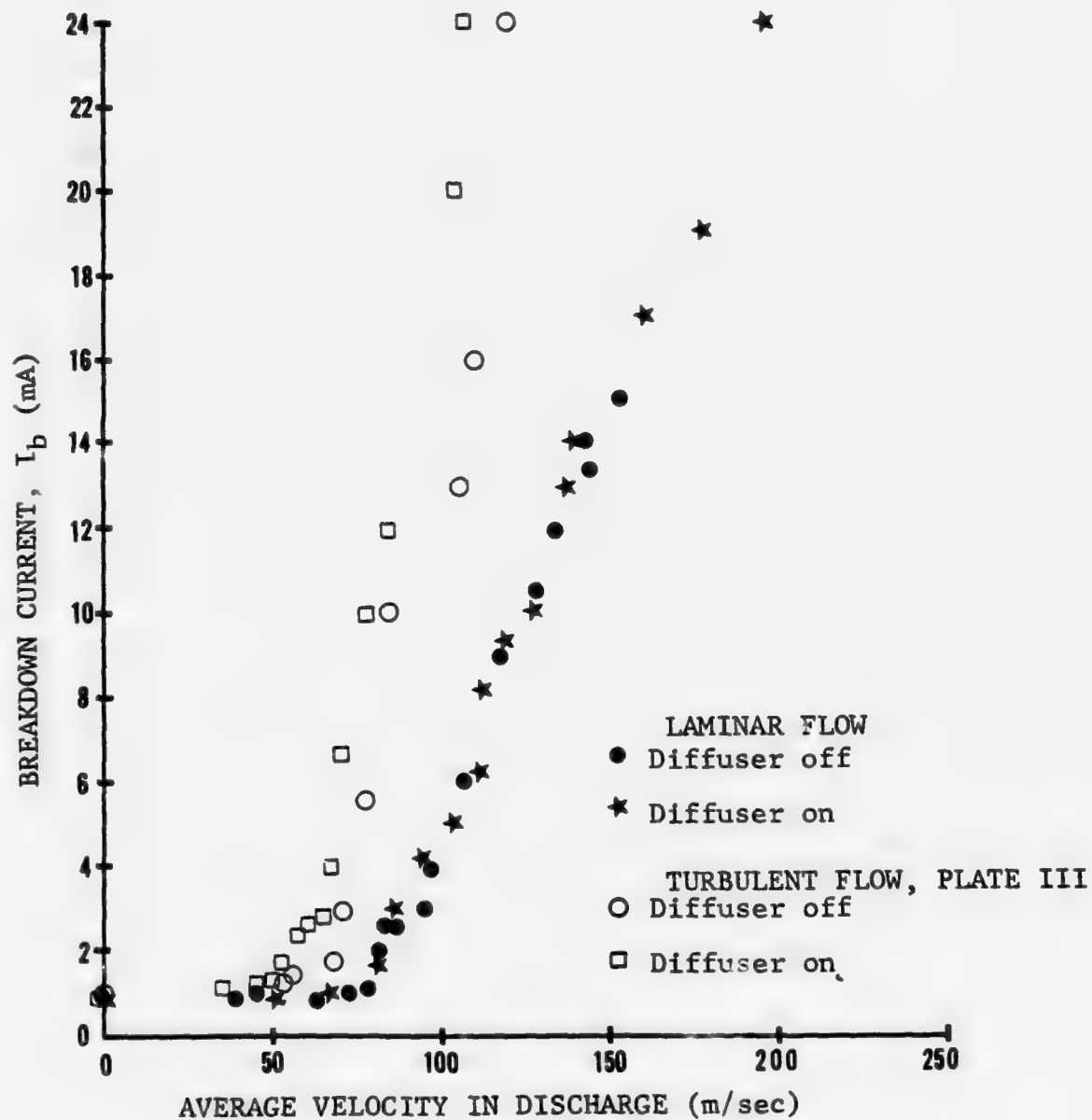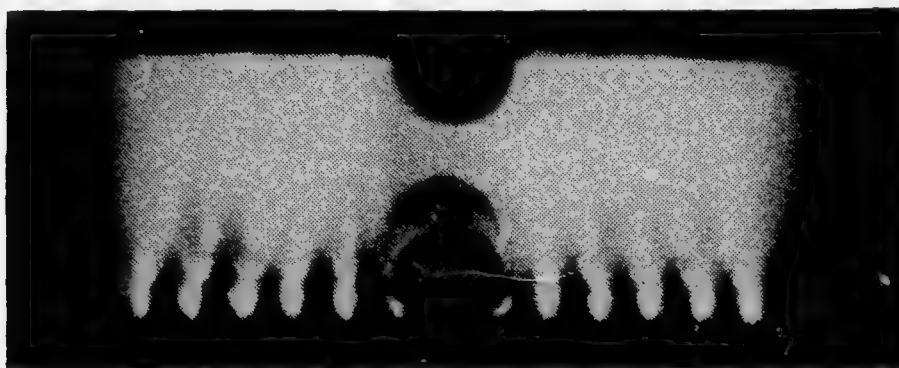Velocity Through the Discharge

46

Figure 18.   Breakdown Current Versus Average
Velocity Through the Discharge

TURBULENT FLOW   LAMINAR FLOW   NO-FLOW
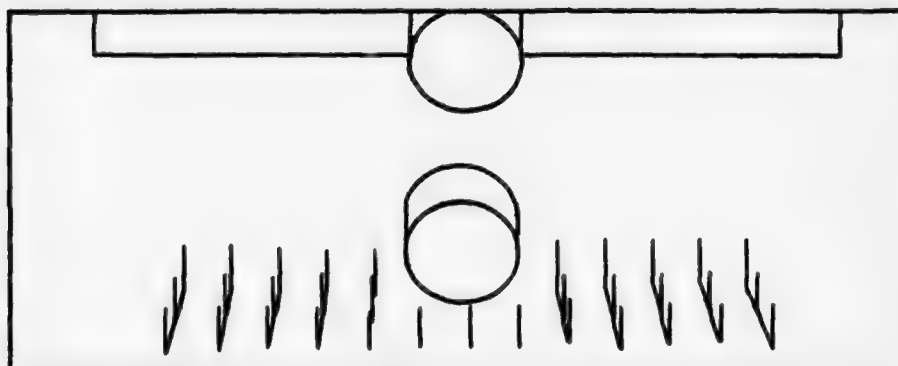
Figure 19.   Discharge Appearance

ANGLE OF VIEW

Anode   Cathode

48

the "laminar" flow photograph, the individual pin dis-
charges were more diffused. An intense, short, narrow
glow extending from the pin anode tips had developed.
This is a region of high current density. As shown in
the turbulent photograph, the discharge had become even
more diffused. The bright region at the tips of each pin
was wider and visibly more dispersed. The localized
current density in this region has become more diffused
due to turbulent mixing. Similar observations are
reported in Reference 3. The outer or periphery pins of
the anode were the first pins to develop the intense bright
region described above. The center pins did not "light
up" as brightly as the outer pins.

VI.   CONCLUSIONS AND RECOMMENDATIONS

Even though maximum operating conditions were not
reached due to power supply current limitations, sub-
ambient, controlled turbulent flow had a significant
effect on discharge stability in the working range of
this experiment. Turbulence generating plates must be
kept in the immediate vicinity of the discharge (location
C, Fig. 3) to avoid spectral decay in a wind-tunnel con-
traction. Power input is scalable with mass flow rate.
The combined effect of reduced pressure and turbulent flow
at maximum performance obtained in this experiment was to
increase discharge power by 750% over ambient laminar
flow at the same mass flow rate.

The upper limit of power input for this apparatus
would occur under choke conditions with Plate III installed
at location C, but a power supply with sufficient output
would be needed to reach that level. The slope of the
turbulent flow curves may or may not eventually decrease
in the same manner as the "laminar" curves, and this
needs to be further investigated. Turbulence spectrum
data could be enhanced by laser velocimeter measurements
of the turbulent flow.

At a given average discharge velocity the total dis-
charge power can be obtained from Figure 16 for either
the turbulent or "laminar" case. This power is represented
by a line of constant power in Figure 15. The intercepts
of this constant power line give mass flow rates correspond-
ing to the diffuser on or off configuration. Since dis-
charge area and velocities are equal, only density accounts
for the difference in mass flow rates. This conclusion
is supported by the data.

By extrapolating the probable path of the "laminar"
curves in Figure 14 (see Fig. 20), decreasing density ratio
versus total discharge power can be projected. The ratio
of mass flow rates corresponding to the intercepts of
constant power lines gives ρ / ρ_o. The resulting curve is
shown in Figure 21.

There are a number of improvements that can be incor-
porated into this apparatus. As mentioned earlier, a
larger power supply would vastly improve the capability of
the system. This would also require additional electric
shielding of the high voltage circuit to protect the
operators. The center row of anode pins had a glow inten-
sity less than the periphery pins for all flow and no-flow
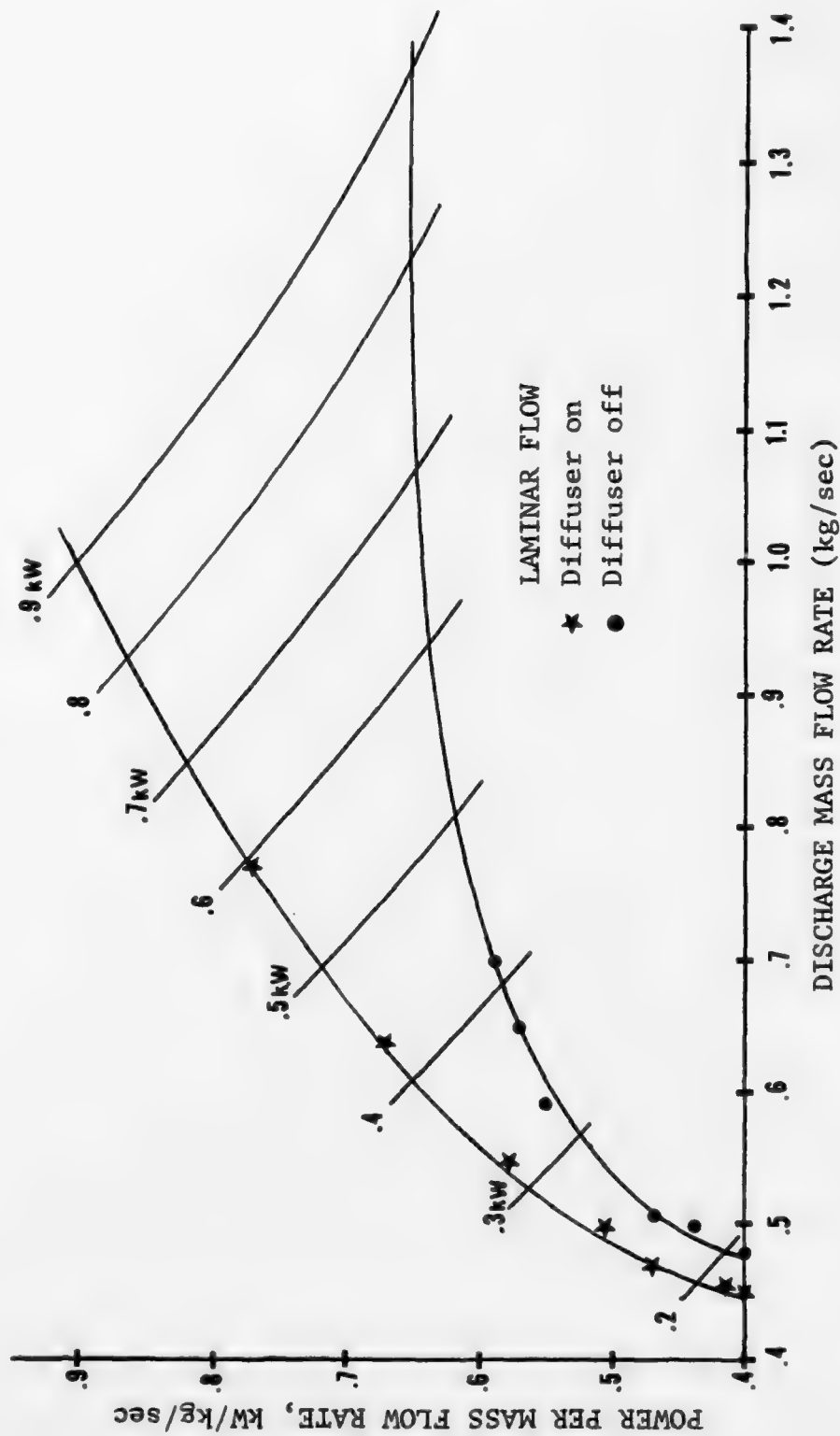tests. This may have been influenced by the cathode wire

51

Figure 20. Extrapolated Laminar Curves

52
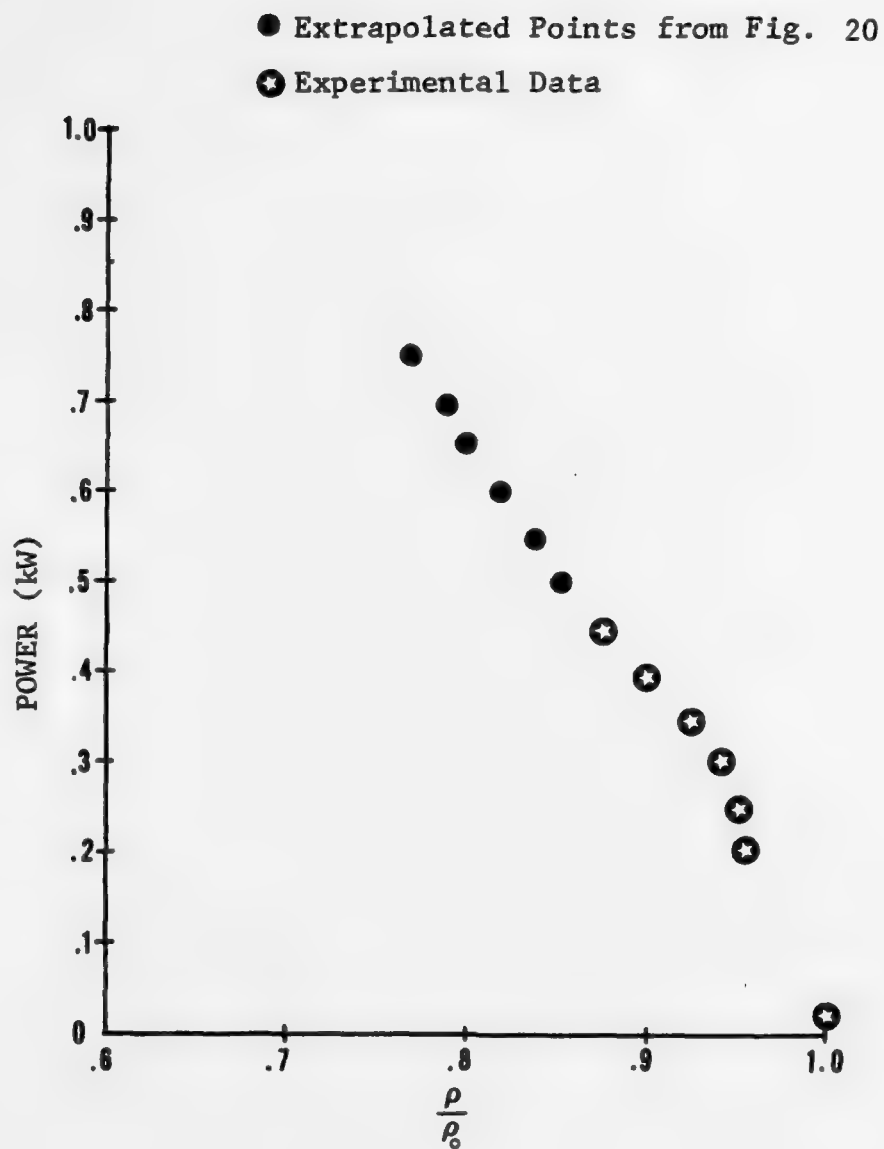
Figure 21.   Power Versus Density Ratio

53

grid frame. Optimizing pin density for turbulent flow may also produce interesting results. An electrode gap length of 2.9 cm was used for all discharge data presented. With a larger power supply the optimum gap for the corresponding operating density of the discharge region could be experimentally determined and improve the performance.

A closed, pressure tight system as suggested by Reference 11 would alleviate the problem of relative humidity and would provide independent control of density and velocity. A closed system would also enable economic use of valuable lasing gas mixtures.

APPENDIX A

PARTIAL PRESSURE OF WATER VAPOR IN DISCHARGE

The relative humidity and temperature of ambient air determines the partial pressure of water vapor at the compressor inlet by using

(1) $P_w = \emptyset P_g$

where P_w is the partial pressure of water vapor, $\emptyset$ is the relative humidity and P_g is the saturation pressure determined from steam tables. A detailed steam table can be found in Reference 14. From Dalton's Law,

(2) $P = P_w + P_a$

where the subscript a refers to the partial pressure of dry air. The specific humidity is given by

(3) $\Gamma = \dfrac{P_w}{P_a} \dfrac{M_w}{M_a} = 0.621 \dfrac{P_w}{P_a} \quad \dfrac{\text{LB OF WATER}}{\text{LB OF AIR}}$

M_w and M_a are the molecular weights of water and air respectively.

From Eqs. (1) and (2), and measured ambient pressure, P_a can be determined, which in turn, when substituted into Eq. (3) will give the specific humidity of the flow. The specific humidity will remain unchanged provided condensation

does not occur. If the flow temperature drops below the local dew point, condensation will take place and, therefore, reduce Γ.

To determine the partial pressure of water vapor in the discharge region, the static pressure and temperature of the test section were measured. Assuming for the present Γ remained constant, Eqs. (2) and (3) are used to determine P_W in the test section.

$$(4) \qquad P_a = \frac{P}{(1 + \Gamma/0.621)}$$

$$(5) \qquad P_W = \frac{P_a}{0.621}$$

The steam tables were used to determine P_g in the test section and substituted into Eq. (1) to determine the relative humidity. If the calculated Φ was greater than or equal to one, Γ had decreased or was about to and the partial pressure of water vapor in the discharge region, P_W, was equal to P_g. If Φ was less than 1, the partial pressure of water vapor as calculated in Eq. (5) was correct.

A corresponding breakdown correction factor was then determined from Figure 22. All data was corrected to standard humidity conditions.
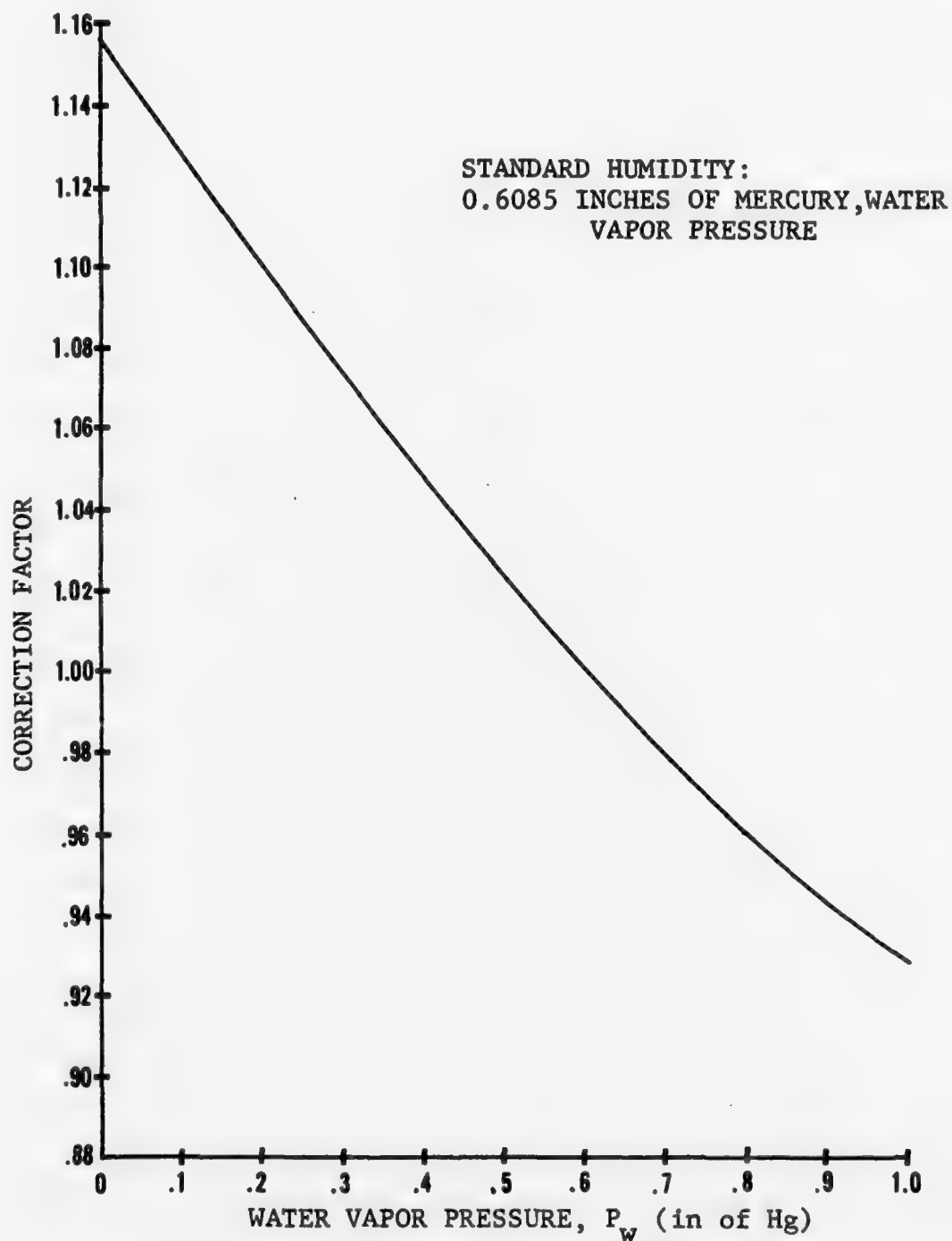
56

Figure 22.   Relative Humidity Correction Curve (Ref. 9)

APPENDIX B

ERROR ANALYSIS (REF. 15)

The uncertainty of the results depended on accurate measurement readings of breakdown voltage and current, total flow temperature and static and stagnation pressures. The following is an estimation of the uncertainty interval of these variables.

Breakdown voltage:

$$V_b = (V \pm 0.2) \ 0.99 \text{ kV}$$

The 0.99 comes from using the control panel voltmeter. Breakdown voltage was first corrected to standard relative humidity.

Breakdown current:

$$I_b = I \pm 0.2 \text{ mA for } 0 < I < 10 \text{ mA}$$

$$I_b = I \pm 1.0 \text{ mA for } 10 < I < 24 \text{ mA}$$

Total Temperature:

$$T_o = T \pm 2 \ ^oR$$

Stagnation Pressure:

$$P_o = p \pm 0.005 \text{ PSIA for } H_2O \text{ manometers}$$

$$P_o = p \pm 0.02 \text{ PSIA for Hg manometers}$$

58

Static Pressure:

$$P_s = p \pm 0.005 \text{ PSIA for } H_2O \text{ manometers}$$

$$P_s = p \pm 0.02 \text{ PSIA for Hg manometers}$$

The intermediate results are functions of the test variables as stated below.

Power:

$$P = VI \text{ watts}$$

Flow Temperature:

$$T = T(T_o, \ p_o, \ p_s) \text{ isentropic}$$

Velocity:

$$v = v(T_o, \ p_o, \ p_s) \text{ isentropic}$$

Density:

$$\rho = \rho(T_o, \ p_o, \ p_s) \text{ isentropic}$$

First, consider the uncertainty in experimental values of power.

    1) $P = VI$ watts

    2) $P + \Delta P = 0.99 \ (V + \Delta V) \ (I + \Delta I)$

Subtracting eq. 1) from 2) gives

$$\Delta P = 0.99 \ (VI + V \ \Delta I + I \ \Delta V + \Delta V \ \Delta I) - 1$$

$$\Delta P = -0.01 \ VI + 0.99 \ (V \ \Delta I + I \ \Delta V)$$

$$\frac{\Delta P}{P} = 0.99 \ (\frac{\Delta I}{I} + \frac{\Delta V}{V}) \quad -0.01$$

59

In a similar manner the uncertainty interval was determined for the remaining test quantities and are summarized below.

Flow Temperature:

$$\frac{\Delta T}{T} = \frac{T_O + \Delta T_O}{\left(\frac{P_O \mp |\Delta P_O|}{P_S \pm |\Delta P_S|}\right)^{0.29}} - 1 \quad , \qquad T \left[{}^O R\right]$$

Velocity:

$$\frac{\Delta v}{v} = \frac{1}{v} \left\{ 12015.08 \, (T_O + \Delta T_O) \left[1 - \left(\frac{P_S \mp |\Delta P_S|}{P_O \pm |\Delta P_O|}\right)^{0.29} \right] \right\}^{0.5} - 1$$

$$v \left[ft/sec \right]$$

Density:

$$\frac{\Delta \rho}{\rho} = \frac{2.70}{\rho} \left[\frac{P_S \pm |\Delta P_S|}{T \mp |\Delta T|} \right] - 1, \qquad \rho \left[\frac{1bm}{ft^3} \right]$$

Mass Flow Rate:

$$\frac{\Delta \dot{M}}{\dot{M}} = \frac{\Delta \rho}{\rho} + \frac{\Delta v}{v}, \qquad \dot{M} \left[\frac{1bm}{sec} \right]$$

LIST OF REFERENCES

1. Fuhs, A. E., unpublished lecture notes from course AE 4505, Laser Technology, given at the Naval Postgraduate School, 1975.

2. Biblarz, O. and Nelson, R. E., "Turbulence Effects of an Ambient Pressure Discharge," Journal of Applied Physics, v. 45, p. 633, Feburary 1974.

3. Wiegand, W. J. and Nighan, W. L., "Influence of Fluid Dynamic Phenomena on the Occurrence of Constriction in cw Convection Laser Discharges," Applied Physics Letter, v. 26, p. 554, 1975.

4. Wasserstron, E., Crispin, Y., Rom, J. and Shwartz, J., The Interaction Between Electrical Discharges and Gas Flow, AIAA Paper 76-315, American Institute of Aeronautics and Astronautics, New York, 1976.

5. Shwartz, J. and Wassertrom, E.,"The Role of Gas Flow and Turbulence in Electric Discharge Lasers," Israel Journal of Technology, v. 13, p. 122-133, May 1975.

6. Loeb, L. B., Electrical Coronas, p. 110, University of California Press, 1965.

7. Barto, J. L., Gasdynamic Effects on an Electric Discharge in Air, MS Thesis, Naval Postgraduate School, Monterey, California, 1976.

8. Tennekes, H. and Lumley, J. L., A First Course in Turbulence, p. 81-84, MIT Press, 1972.

9. Cobine, J. D., Gaseous Conductors, Theory and Engineering Applications, p. 181-183, McGraw-Hill, 1941.

10. Phelps, C. T. and Griffiths, R. J., "Dependence of Positive Corona Streamer Propagation on Air Pressure and Water Vapor Content," Journal of Applied Physics, v. 47, p. 2929, July 1976.

11. Aunchman, L. J. Jr., <u>Controlled Turbulence as a Design Criterion for Electric Discharge Convection Lasers</u>, MS Thesis, Naval Postgraduate School, Monterey, California, March 1974.

12. Shapiro, A. H., <u>The Dynamics and Thermodynamics of Compressible Fluid Flow</u>, v. 1, p. 83-87, Ronald Press, 1953.

13. Shih, C. C., (private communication).

14. Smithsonian Meteorological Tables, 6th ed., p. 351-359, Smithsonian Institution, 1951.

15. Miller, J. A., unpublished lecture notes from course AE 2806, <u>Aeronautical Labs II</u>, given at the Naval Postgraduate School, 1975.